Supporting Information

Length-Dependent Plasmon Resonance in Single-Walled Carbon Nanotubes

Takahiro Morimoto,[1] Soon-Kil Joung,[1] Takeshi Saito,[1,2] Don N. Futaba,[1,2] Kenji Hata,[1,2] and Toshiya Okazaki[1,2]

[1]Technology Research Association for Single Wall Carbon Nanotubes (TASC), Tsukuba 305-8565, Japan

[2]Nanotube Research Center, National Institute of Advanced Industrial Science and Technology (AIST), Tsukuba 305-8565, Japan

FIR spectroscopic characterization on e-DIPS, HiPco and super-growth (SG) SWCNTs

1. e-DIPS-SWCNTs

Figure S1(a) shows the histograms of length distributions of the e-DIPS-SWCNTs [1] after several different sonication processes (top to bottom:10 min, 20 min, 1 h and 2 h), as estimated from AFM observations. As increasing the sonication time, the average tube length decreases from 1.04 μm to 0.58 μm. Figure S1(b) shows the resonance Raman spectra of the processed samples. A prominent peak of the radial breathing mode (RBM) was observable at around 98-145 cm^{-1}, which corresponds to a diameter of d_t ~1.7-2.5 nm [2]. It can be clearly seen that the RBM shapes and peak positions are nearly identical for all sonication processes. Figure S1(c) shows the optical absorption spectra of the SWCNT samples with different sonication time. In the energy region, the first and second interband transitions for the semiconducting SWCNTs (S1 and S2) were observed at ~2400 nm and ~1320 nm, respectively. The peak positions and the spectral shapes are apparently insensitive to sonication duration time. The absence of any significant change in either the Raman spectrum or the absorption spectrum strongly suggests that the diameter and chiral angle distributions of the e-DIPS-SWCNTs remained unchanged throughout all sonication processes.

The optical response in the FIR region shows significant sonication-time dependence. Figure S2 is the FIR absorption spectra of the e-DIPS-SWCNTs with different sonication times from 10 min to 2 h. Apparently, as increasing the sonication time, the FIR peak position shifts towards higher frequency from ~80 cm^{-1} to ~320 cm^{-1}. Because the diameter and chiral-angle distributions are unchanged (Fig. S1(b),(c)), the observed shifts are unambiguously caused by the shortening in the tube length (Fig. S1(a)).

2. HiPco-SWCNTs

Figure S3(a) shows the histograms of the length distributions of the HiPco-SWCNTs after several different sonication processes (top to bottom: 10 min, 20 min, 1 h and 2 h), as estimated from AFM observations. As increasing the sonication time, the average tube length decreases from 0.79 μm to 0.48 μm. Figure S3(b) shows the resonance Raman spectra of the processed samples. A prominent peak of the RBM was observable at around 220-290 cm^{-1}, which corresponds to a diameter of d_t ~0.8-1.1 nm [2]. It can be clearly seen that the RBM shapes and peak positions are almost identical during the sonication processes. Figure S3(c) shows the optical absorption spectra of the SWCNT

samples with different sonication time. In these energy region, the S1 and S2 transitions for the semiconducting SWCNTs and the M1 transition for metallic SWCNTs were observed at 1000-1300 nm, 650-810 nm and 460-600 nm, respectively. The overall spectral features are apparently insensitive to sonication duration time. The absence of any significant change in either the Raman spectrum or the absorption spectrum strongly suggests that the diameter and chiral-angle distributions of the HiPco SWCNTs remained unchanged throughout all sonication processes.

The optical response in the FIR region shows significant sonication-time dependence. Figure S4 is the FIR absorption spectra of the HiPco-SWCNTs with different sonication times from 10 min to 2 h. Apparently, as increasing the sonication time, the FIR peak position shifts towards higher frequency from ~160 cm^{-1} to ~320 cm^{-1}. Because the diameter and chiral-angle distributions are unchanged (Fig. S3(b),(c)), the observed shifts are unambiguously caused by the shortening in the tube length (Fig. S3(a)).

3. SG-SWCNTs

Figure S5(a) shows the histograms of the length distributions of the SG-SWCNTs [3] after several different sonication processes (top to bottom: 3 min, 10 min, 30 min. and 1 h), as estimated from AFM observations. As increasing the sonication time, the average tube length decreases from 0.40 μm to 0.33 μm. Figure S5(b) shows the resonance Raman spectra of the processed samples. A prominent peak of the radial breathing mode (RBM) was observable at around 167-306 cm^{-1}, which corresponds to a diameter of d_t ~0.8-1.48 nm [2]. It can be clearly seen that the RBM shapes and peak positions are nearly identical for all sonication processes. The S1 transition of SG-SWCNT were observed at 2340 cm^{-1} (= ~4270 nm) in the FIR spectra (Fig. S6). Even though the signals locate at shoulders of the FIR spectra, the peak positions and the spectral shapes are apparently insensitive to sonication duration. The absence of any significant change in either the Raman spectrum or the absorption spectrum strongly suggests that the diameter and chiral-angle distributions of the SG-SWCNTs remained unchanged during throughout all sonication processes.

The optical response in the FIR region shows significant sonication-time dependence (Fig. S6). As increasing the sonication time, the FIR peak position shifts towards higher frequency from ~360 cm^{-1} to ~410 cm^{-1}. Because the diameter and chiral-angle distributions are unchanged, the observed shifts are unambiguously caused by the shortening in the tube length.
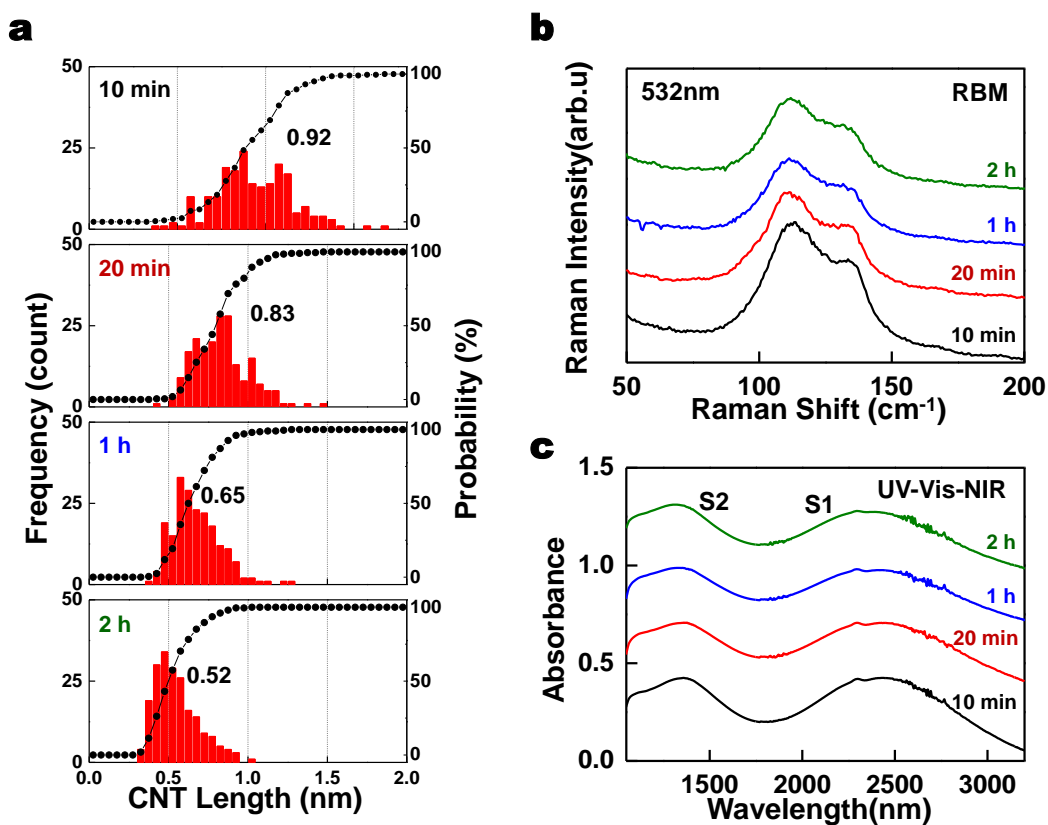
Figure S1. (a) Tube-length distribution of e-DIPS-SWCNTs based on AFM observations. Each panel shows the results for samples that correspond to different sonication times: from top to bottom, the sonication time was 10 min, 20 min, 1 h and 2 h. The numbers inside the panels denote the median values of the distributions. (b) Resonance Raman and (c) UV-Vis-NIR absorption spectra of e-DIPS-SWCNTs with different sonication times. The baselines of the spectra are adjusted.
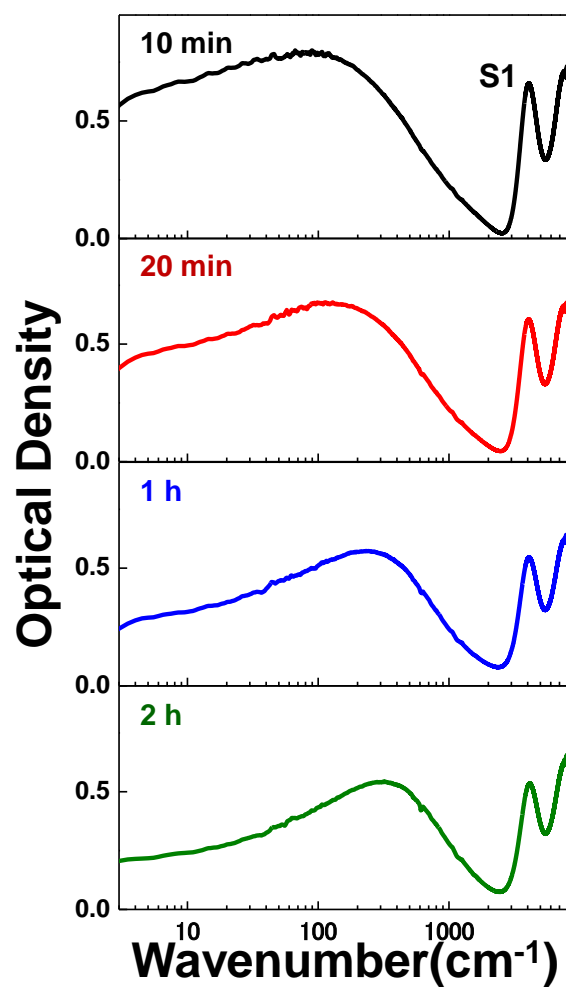
Figure S2. FIR spectra of e-DIPS-SWCNTs with different sonication times of 10 min, 20 min, 1 h and 2 h (from top to bottom). The sharp peaks near 4000 cm^{-1} correspond to the S1 interband transition.
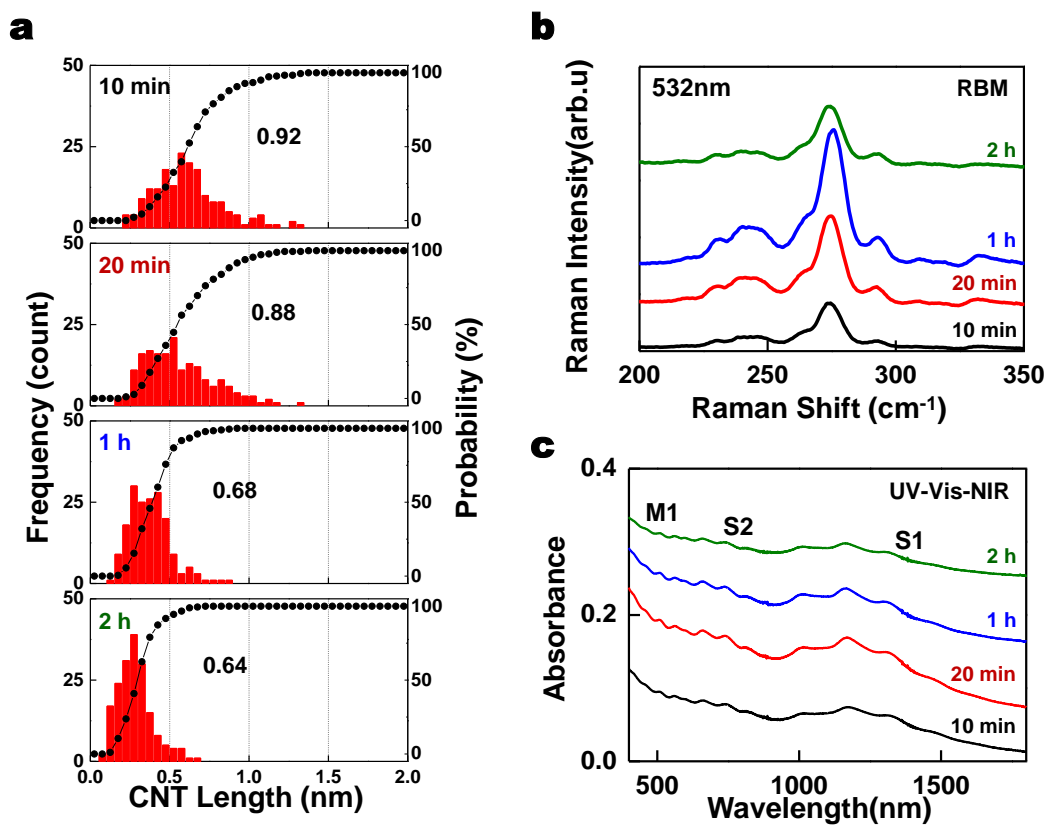
Figure S3. (a) Tube-length distribution of HiPco-SWCNTs based on AFM observations. Each panel shows the results for samples that correspond to different sonication times: from top to bottom, the sonication time was 10 min, 20 min, 1 h and 2 h. The numbers inside the panels denote the median values of the distributions. (b) Resonance Raman and (c) UV-Vis-NIR absorption spectra of HiPco-SWCNTs with different sonication times. The baselines of the spectra are adjusted.
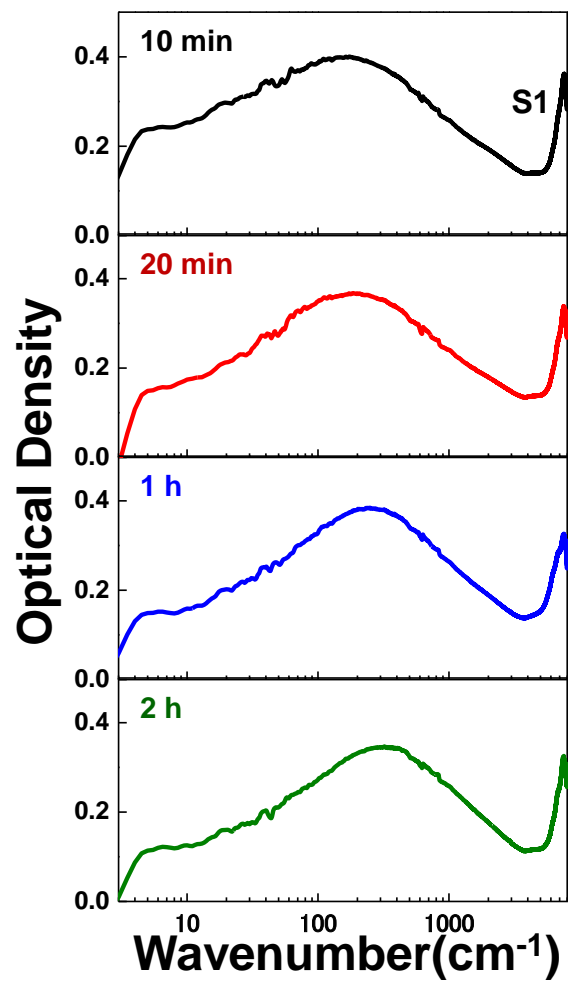
Figure S4. FIR spectra of HiPco-SWCNTs with different sonication times of 10 min, 20 min, 1 h and 2 h (from top to bottom). The shoulders of the S1 peaks can be seen at around 7000 cm^{-1}.
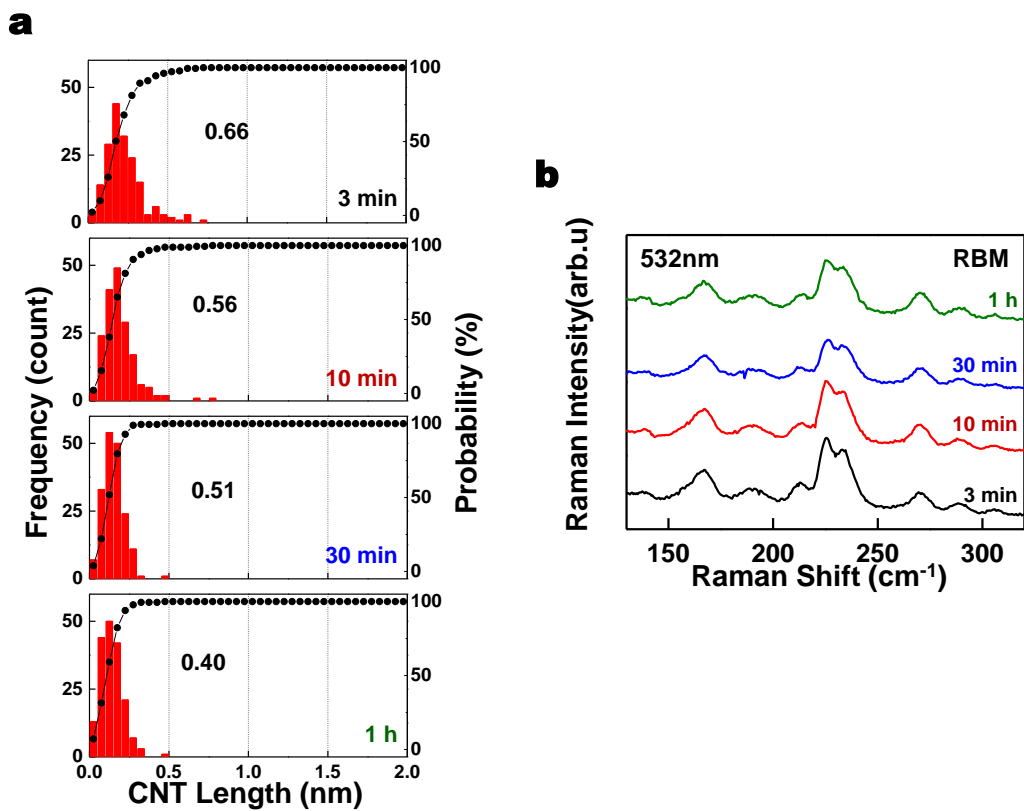
Figure S5. (a) Tube-length distribution of SG-SWCNTs based on AFM observations. Each panel shows the results for samples that correspond to different sonication times: from top to bottom, the sonication time was 3 min, 10 min, 30 min. and 1 h. The numbers inside the panels denote the median values of the distributions. (b) Resonance Raman spectra of SG-SWCNTs with different sonication times.
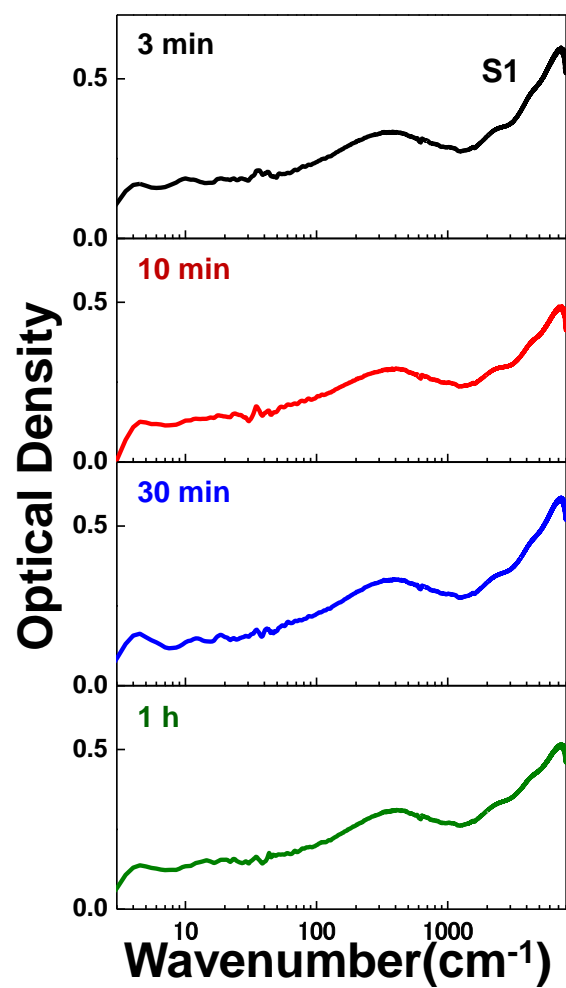
Figure S6. FIR spectra of SG-SWCNTs with different sonication times of 3 min, 10 min, 30 min and 1 h (from top to bottom). The small peaks at around 2340 cm^{-1} correspond to the S1 interband transition.

TCNQ doping results on separated arc-SWCNTs.

Figures S7(a) and (b) show the UV-Vis-NIR spectra of metallic-rich (M-arc) and semiconducting-rich (S-arc) arc-SWCNTs before and after doping with TCNQ. Before doping, the sample films were annealed in vacuum (600 ºC, ~10^{-5} Pa for 1 h) to remove adsorbed molecules such as oxygen and water. Both samples show clear interband excitation peaks at ~1800 nm, ~1000 nm and ~700 nm, corresponding to the S1, S2 and M1 transitions, respectively (red lines in Fig. S7(a),(b)). Upon TCNQ doping, these peaks are suppressed by the hole injection to the van Hove singularities in the valence bands (blue lines in Fig. S7(a),(b)). It should be noted that the suppression is smaller than that in the case of the F_4TCNQ doping.

Figure S7(c) and (d) show the effects of the doping on the FIR spectra of the M-arc and S-arc samples. The red and blue lines denote the spectra before and after doping, respectively. The spectral intensities were normalized to the sample thicknesses that were estimated from AFM observations. Upon TCNQ doping, the signal intensities of both M-arc and S-arc samples are enhanced as is the case of F_4TCNQ (Fig. 4). The different enhancement behavior between M-arc and S-arc samples is discussed in the text.
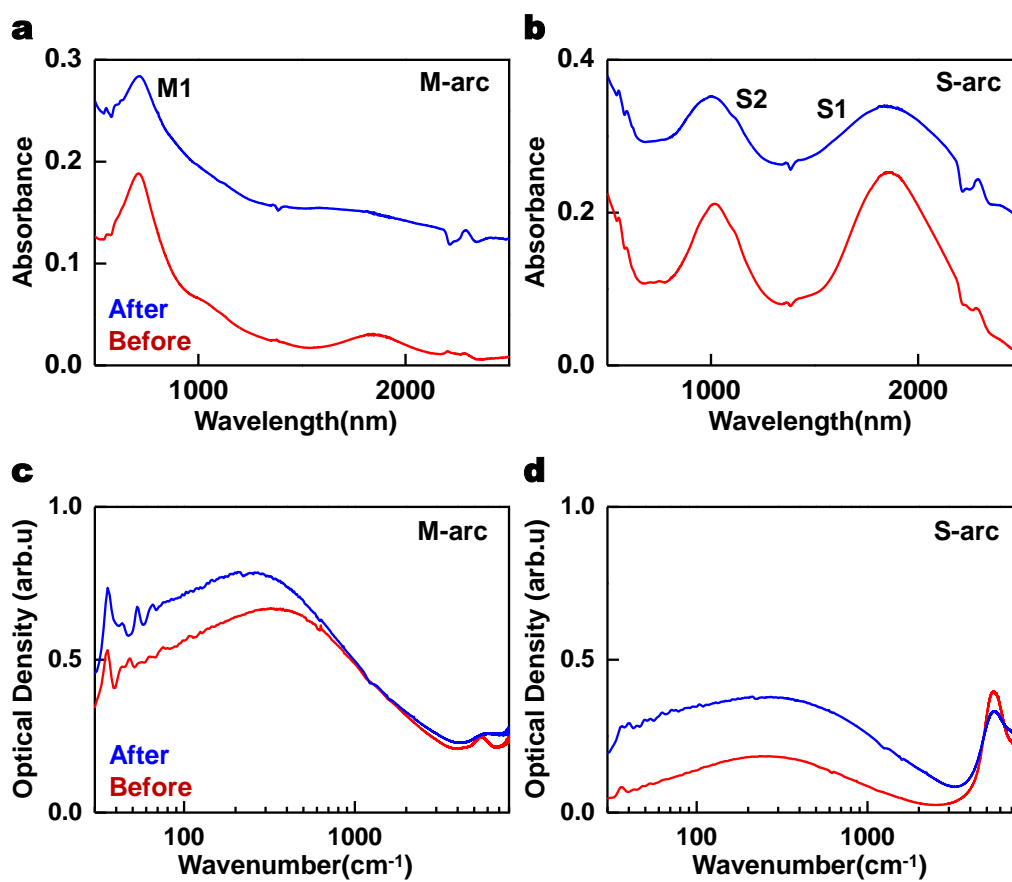
Figure S7. (a), (b) UV-Vis-NIR and (c), (d) FIR spectra of (a), (c) metallic and (b),(d) semiconducting enriched arc-SWCNT samples. The red and blue lines are the spectra before and after TCNQ doping, respectively.

Resonance Raman spectra of as-received SWCNTs in G- and D-modes region

Figure S8 shows the resonance Raman spectra of SWCNTs with the short sonication times. The G/D ratios are calculated from the areas of the G- and D-modes by the curve fitting with Lorentz functions. Excitation wavelength is 532 nm.
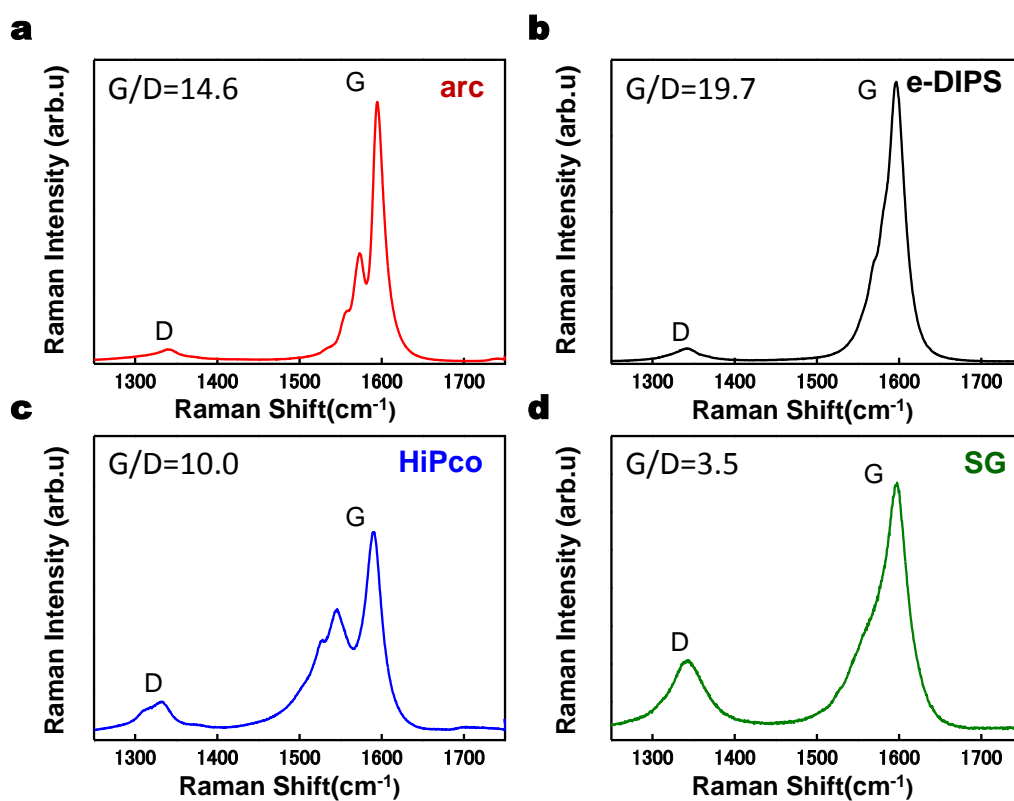

Figure S8. Resonance Raman spectra of (a) arc-, (b) e-DIPS-, (c) HiPco- and (d) SG-SWCNTs in the region of G- and D-modes.

References in Supporting Information

1. Saito, T.; Ohshima, S.; Okazaki, T.; Ohmori, S.; Yumura, M.; Iijima, S. Selective Diameter Control of Single-Walled Carbon Nanotubes in the Gas-Phase Synthesis, *J. Nanosci. Nanotechnol.* **2008**, *8*, 6153-6157.

2. Rao, A. M.; Richter, E.; Bandow, S.; Chase, B.; Eklund, P. C.; Williams, K. A.; Fang, S.; Subbaswamy, K. R.; Menon, M.; Thess, A. *et al.* Diameter-Selective Raman Scattering from Vibrational Modes in Carbon Nanotubes. *Science*, **1997**, *275*, 187-191.

3. Hata, K.; Futaba, D. N.; Mizuno, K.; Namai, T.; Yumura, M.; Iijima, S. Water-Assisted Highly Efficient Synthesis of Impurity-Free Single-Walled Carbon Nanotubes. *Science* **2004**, *306*, 1362-1364.